Anal. Bioanal. Electrochem., Vol. 16, No. 10, 2024, 957-966
https://www.doi.org/10.22034/abec.2024.717552

Analytical & Bioanalytical Electrochemistry

Full Paper

Electrochemical Synthesis of An Effective Bifunctional MOF Catalyst for Oxygen Reduction Reaction in Alkaline Media

Asma Bananezhadand, and Mohammad Reza Ganjali*

Center of Excellence in Electrochemistry, School of Chemistry, College of Science, University of Tehran, Tehran, Iran

*Corresponding Author, Tel.: +98-21-88356145
E-Mail: ganjali@ut.ac.ir

Received: 14 April 2024 / Received in revised form: 25 September 2024 / Accepted: 11 October 2024 / Published online: 31 October 2024

Abstract- A nickel/copper benzene-1,3,5-tricarboxylate metal-organic framework (MOF) was prepared through a rapid and effective electrochemical process. The properties of the obtained catalyst were studied with Fourier-transform infrared spectroscopy (FTIR), thermal gravimetric analysis (TGA), and X-ray powder diffraction (XRD). The electrocatalytic behavior of the synthesized catalyst in an oxygen reduction reaction (ORR) was studied with a rotating disk electrode in alkaline media and compared to the catalytic behavior of a platinum commercial catalyst at the same conditions. A comparison of the obtained results showed that the synthesized catalyst showed more current density and positive onset potential than the commercial platinum catalyst in ORR. This work introduces an effective and rapid electrochemical synthesis of high-porosity MOF compounds for advanced electrocatalytic applications.

Keywords- Bi-functional electrocatalyst; Electrochemical synthesis; Metal-organic framework; Platinum-free catalysts; Oxygen reduction reaction (ORR)

1. INTRODUCTION

Increasing attention to environmental pollution control and the growing need for energy has focused much research on the study of different types of energy transformation systems (ETS) and sustainable storage devices like fuel cells, rechargeable metal-air batteries, and water splitting [1–3]. Oxygen reduction reaction (ORR) and oxygen evolution reaction (OER)

are two crucial electrochemical reactions in these systems. These reactions are corresponding to the charge and discharge processes via multi-electron transfer processes with various reaction mechanisms and different intermediates [4]. In recent years, great efforts have been made to expand exceptionally efficient catalysts for OER and ORR. In the contemporary era of technology, platinum (Pt) based substances are the most sensible catalysts. Especially, the Pt/C catalyst has demonstrated brilliant catalytic behavior for ORR [5-7].

Because Pt-based catalysts are too highly priced to prepare commercially feasible metallic-air batteries, during the last several long-time extensive studies have centered on expanding alternative catalysts, inclusive of non-noble metal catalysts [8]. Some of these materials are perovskite oxide catalysts [9], transition metallic oxides [10,11], carbon nanotube-supported nanoparticles [12], spinel oxides [13,14], enzymes [15] and Metal-organic frameworks [16,17].

Recently, metal-organic frameworks (MOFs) as a unique category of porous substances have been developed in scientific research. These compounds are crystalline, and in their chemical structures, metallic ions and multidentate organic ligands are joined collectively via coordinate bonds, so they are organic-inorganic hybrid substances. MOFs show large effective surface areas with the ability to adjust the size of the pores and functionality. Also, MOFs show more catalytic behavior than metallic oxides. In this material the shape-to-size ratio is selectable. They can act as hosts for a large group of guest molecules [18]. MOFs have attracted much attention due to their various uses in numerous studies and different fields for example; gas storage and separation [19, 20], magnet [21], drug delivery [22,23], sensing [24], energy storage [25] and catalysis [26].

MOFs are fascinating and beneficial in electrochemical research. Because MOFs are commonly successive metal complex units, depending on the metal ions and type of ligands can be electrochemically active [27]. Hence, MOFs can display promising electrocatalytic activity for ORR. Solvothermal synthesis, microwave-assisted, mechanochemical, sonochemical, and electrochemical synthesis are common ways to synthesize MOFs [28]. Among these ways, electrochemical synthesis is a useful method in many environments because it is a metal salt-free and continuous production process. One of the major benefits of synthesis by the electrochemical process is mild synthesis conditions in comparison with solvothermal or microwave methods. Also, while synthesis by solvothermal method takes hours or days, the electrochemical synthesis will manufacture MOFs generally within some minutes [29-32].

Herein, we synthesize a bifunctional MOF through a fast, simple, and economical electrochemical method. We used a cathodic electro-syntheses (CES) system for the manufacture of a bimetallic MOF based on an organic linker, BTC (BTC = benzene 1,3,5 tricarboxylate), nickel chloride, and copper chloride as Ni(II) and Cu(II) sources. The Ni/Cu-BTC-MOF was successfully ready and employed in the ORR analyses. The electrocatalytic behavior of the synthesized MOF was studied and the obtained results were compared to the

commercial platinum catalyst (Platinum on carbon (Pt /C)) for ORR reaction in alkaline media. According to the results the Ni/Cu-BTC-MOF displayed more current density and positive onset potential than Pt /C catalyst in ORR.

2. EXPERIMENTAL SECTION

2.1. Materials

All precursors materials for the preparation of the catalyst including Nickel(II) chloride hexahydrate ($NiCl_2{\cdot}6H_2O$), Copper(II) chloride dihydrate ($CuCl_2{\cdot}2H_2O$), benzene-1,3,5-tricarboxylic acid (H_3BTC, 95%), sodium nitrate ($NaNO_3$, 99%), nafion solution (5 wt. %), methanol (MeOH) and ethanol (EtOH, 96%) were purchased from Sigma-Aldrich company. 20% wt. Pt/C was bought from the Matthey Johnson company. All of the chemicals were used without any purification.

2.2. Electrocatalyst Synthesis

The cathodic electro-syntheses (CES) system was applied for the synthesis of MOFs. The method used a two-electrode system including a stainless-steel foil with dimensions of 2.5 cm × 2.5 cm located between two graphite disks (with an area of 5 cm × 5 cm) as anodes. This setup was similar to our previous work [33]. According to our previous work, $NiCl_2{\cdot}6H_2O$ (0.15 mg), $CuCl_2{\cdot}2H_2O$ (0.05 mg), $NaNO_3$ (0.05 g), and H_3BTC (0.1 g) were dissolved in 200 ml EtOH and used as a bath for deposition. The optimum conditions for deposition are as follows; be i = 1 A/dm^2, $t_{deposition}$ = 10 min, pH = 6.5 and T_{bath} = 25 ºC. After the end of deposition time, the steel foil was removed from the deposition bath, and washed several times with EtOH. The formed precipitate was then separated from the foil. Then, the formed precipitate was removed from the foil and dried for 2h at 70 ºC temperature. The resulting powder was Ni/Cu-BTC-MOF.

2.3. Structural characterization

The Fourier-transform infrared (FTIR) spectra of the Ni/Cu-BTC-MOF were recorded in the range of 400-4000 cm^{-1} by a Shimadzu S8400 FT-IR spectrophotometer. To understand the details about the crystal structure of the Ni/Cu-BTC-MOF catalyst, an X-ray diffraction pattern was reported at 25 °C by a Phillips PW-1800 diffractometer with Cu Kα radiation. The thermal stability of the Ni/Cu-BTC-MOF was evaluated by a Thermo Gravimetric Analyzer (TGA Q50) up to 500 °C.

2.4. Electrochemical measurements

For electrochemical evaluation, a general three-electrode system with potassium hydroxide (KOH, 0.1 mol L^{-1}) solution as the electrolyte was used. A rotating disk electrode (Glassy

carbon working electrode 5 mm) was used as the working electrode. The Ag /AgCl/$KCl_{sat.}$ electrode and Pt wire have been used as reference and auxiliary electrodes, respectively. The active sample (5 mg) was dispersed in a mixed solution of water/ethanol (1 mL, 1:1 (V/V)) containing 30 μmol L^{-1} of nafion solution (5 wt.%) through ultra-sonication for about 2 hours to eventually create a homogeneous ink. Then a specified and optimized volume (20 μmol L^{-1}) of ink was pipetted on the GCE surface. The synthesized electrocatalyst was dried on the electrode surface at room temperature and used as the working electrode for electrochemical measurements. The yield of the electrocatalyst was obtained 0.15 mg cm^2. The results were compared with the Pt/C catalyst. To carry out the test of ORR, the electrolyte (KOH) was purged with oxygen gas (high-purity) at a constant flow rate (50 mL min^{-1}) for 1 hour to ensure oxygen saturation. Also to create an oxygen-free environment was used nitrogen gas. The cyclic voltammetry (CV) analysis was conducted by scanning the potential from 0.3 to -0.9 V *vs*. Ag/AgCl, with a scan rate of 50 mV s^{-1}. The linear sweep voltammetry (LSV) measurements were conducted at the same range of potential (0.3 to -0.9 V *vs*. Ag/AgCl) at electrode rotation rates of 400, 800, 1200, 1600, and 2000 rpm with a scan rate of 10 mV s^{-1}. To determine the kinetic parameters of the ORR tests, the Koutecky-Levich equation (Eq. 1) was used [33]:

$$\frac{1}{j} = \frac{1}{j_k} + \frac{1}{j_d} = \frac{1}{nFkC_{O2}} + \frac{1}{0.62nFC_{O2}D_{O2}^{2/3}v^{-1/6}\omega^{1/2}} \quad (1)$$

where; j_k and j_d are the kinetic and the diffusion-limiting current density (mA cm^{-2}), j is the measured disk current density (mA cm^{-2}), n is the electron transfer number in the ORR pathway, F is the Faraday constant (96,485 C mol^{-1}), C_{O2} is the O_2 concentration in 0.1 mol L^{-1} KOH electrolyte (1.26×10^{-6} mol cm^{-3}), D_{O2} is the O_2 diffusion coefficient in KOH electrolyte (1.93×10^{-5} cm^2 s^{-1}), v is the kinematic viscosity of 0.1 mol L^{-1} KOH electrolyte (1.09×10^{-2} cm^2 s^{-1}), and ω is the rotation rate of RDE (rad s^{-1}).

3. RESULTS AND DISCUSSION

3.1. Morphology and characterization

Ni/Cu-BTCMOF crystalline powders were manufactured through electrochemical reactions among organic ligand (H_3BTC) and Ni(II) and Cu(II) salt solutions at ambient temperature. For the structure of Ni/Cu-BTC MOF was proposed a special conjugation system involving *d*-orbital (*metal)*-π (BTC) interactions [34]. The synthesized electrocatalyst FT-IR spectrum is displayed in Figure 1a. The broad adsorption band at 3456 cm^{-1} was related to (O–H) stretching vibrational band from physically adsorbed or coordinated H_2O. The peak observed at 1450 cm^{-1} was attributed to the symmetric vibration of the carboxylic group, while the asymmetric vibration bands of the carboxylic group appeared in 1565 and 1515 cm^{-1}. The absence of the absorption peak corresponding to the hydroxyl (–COOH) group between 1730 cm^{-1} and 1690 cm^{-1} confirmed the de-protonation of H_3BTC when it is linked to metal ions. It

should also be noticed after doping of Ni and Cu ions the stretching vibrational bands Cu–O and Ni–O appear in 750 and 460 cm^{-1}, respectively. According to the FTIR analysis, the synthesis of the Ni/Cu-BTC-MOF can be confirmed. Figure 1b shows the XRD pattern of the synthesized electrocatalyst. The position of the diffraction peaks in this pattern is the same as that reported in previous research [35]. The X-ray diffraction analysis cannot easily distinguish between Cu and Ni ions in the units of the framework. This is due to the close ionic radius of the Ni (II) and Cu (II) and the similar electron density in these two ions. Therefore, it can be concluded that the catalyst synthesis is well performed [36]. TGA analysis of Ni/Cu-BTC-MOF can be seen in Fig. 1c. Three levels of weight loss are mentioned for Ni/Cu-BTC-MOF. The first and second weight loss levels at about 80 ºC and 300 ºC are related to the physically and chemically absorbed H_2O in the structure of Ni/Cu-BTC-MOF, respectively. The third level at 375 ºC is related to the removal of the linker (BTC) and then the decomposition of the Ni/Cu-BTC-MOF structure

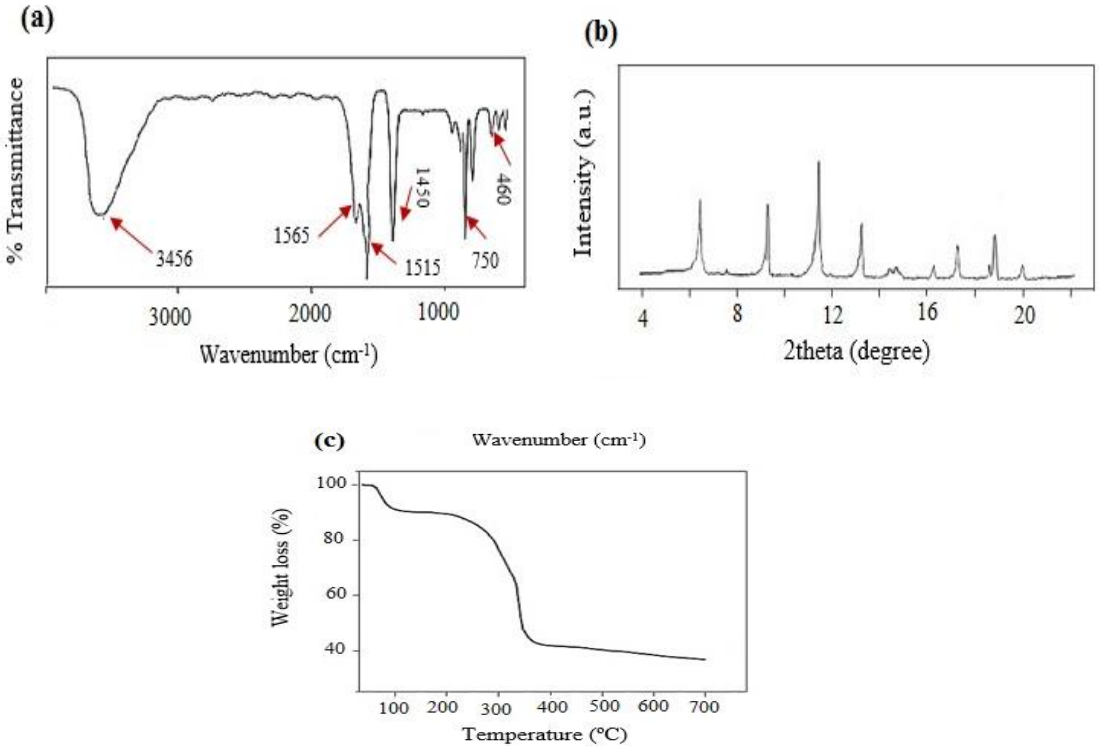

Figure 1. FT-IR spectrum (a), XRD pattern (b), TGA graph (c)

3.2. Electrochemical analysis

The electrochemical tests were performed to study the electrocatalytic performance of the Ni/Cu-BTC-MOF in alkaline electrolytes using RDE for ORR. To determine the basic electrocatalytic efficiency of Ni/Cu-BTC-MOF for ORR, CV analysis was performed in N_2 and O_2-saturated KOH solution from 0.3 V to -0.9 V (*vs*. Ag / AgCl) at a scan rate of 50 mV s^{-1}. Regarding the geometrical area, the current densities have all been normalized. According to

Figure 2a, the modified electrode with Ni/Cu-BTC-MOF displays no peak in the electrolyte saturated with N_2 gases. While an excellently-defined and strong peak was observed in O_2 saturated electrolyte at -0.3 V (*vs* Ag/AgCl), which represents good behavior of Ni/Cu-BTC for ORR. The LSV analysis was performed in O_2 saturated KOH solution at a scan rate of 10 mV s^{-1} and a rotation rate of 1600 rpm. The results are seen in Figure 2b. Table 1 lists quantitative data such as onset potential, half-wave potential, and current density for ORR on modified electrode. As well as data have been compared with the results obtained from the 20% wt. Pt/C. The results indicate the excellent efficiency of Ni/Cu-BTC-MOF in the metal-air batteries for catalyzing the ORR reaction. According to the result, can be said, the combination of two characteristics of porosity and nano size of materials can successfully shorten ion transfer pathways and enhance active areas, thus greatly enhancing the electrical conductivity of the materials to enhance its catalytic ORR activities. The results of this study are comparable to the recent published for example; Co-4,4′-Oxybis (benzoic acid)/C catalyst [37], Co@CoO@Co_3O_4-N/C [38], Co/N-doped porous carbon fibers [39], C-Fe-Z8-Ar [40], Pt-CeO_2-C [41], Fe_3C@NC [42] and Co–N–C porous nanocomposite [43].

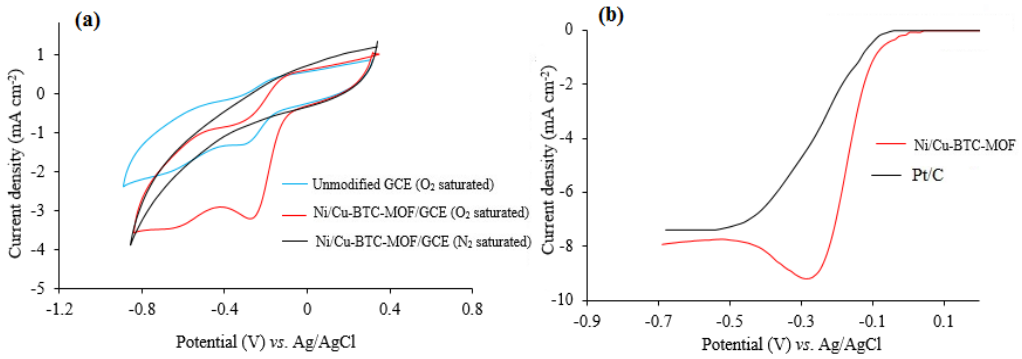

Figure 2. (a) CV curves of the unmodified GCE, Ni/Cu-BTC-MOF catalyst in an N_2 and O_2-saturated in 0.1 mol L^{-1} KOH at a scan rate of 50 mV s^{-1} (b) ORR polarization curves of the Ni/Cu-BTC-MOF and high-quality commercial 20 wt.% Pt/C catalysts in an O_2-saturated 0.1 mol L^{-1} KOH with a sweep rate of 10 mV s^{-1} at a rotation speed of 1600 rpm at room temperature

Table 1. Summary of electrocatalytic properties for Ni/Cu-BTC-MOF and 20 wt. % Pt/C catalysts

Sample	**Eonset [a] / V**	**$E_{1/2}$ / V**	**|j| [b] / mA cm^{-2}**	**Electron transfer number (n)**
Ni/Cu-BTC-MOF	0.0	-0.156	8.0	3.7-3.9
20 wt. % Pt/C	-0.08	-0.25	7.4	4

[a] Onset potential was acquired at an ORR current density of 0.1 mA cm^{-2}
[b] Limiting current density was obtained at -0.6 V vs. Ag/AgCl/$KCl_{sat.}$

Figure 3a shows the LSV curves of Ni/Cu-BTC-MOF for the ORR at different rotation speeds. As it is seen, the current densities are enhanced with rising the rotation rates of working electrode. Fig. 3b shows the corresponding Koutecky Levich curves derived from the inverse current density (j^{-1}) as a function of the inverse of the square root ($\omega^{-1/2}$) for modified electrodes at specified potentials. The graphs are approximately linear and parallel, which shows the first-order dependency of the kinetics of the ORR at the surface of the modified electrode. According to equation 1, the number of transferred electrons in the oxygen reduction pathway was determined to be approximately 3.8 (Fig. 3c). This value is near to the theoretical value of direct $4e^-$ ORR. Therefore, it can be concluded that the ORR on the synthesized catalyst took place via the most effective $4e^-$ reduction pathway.

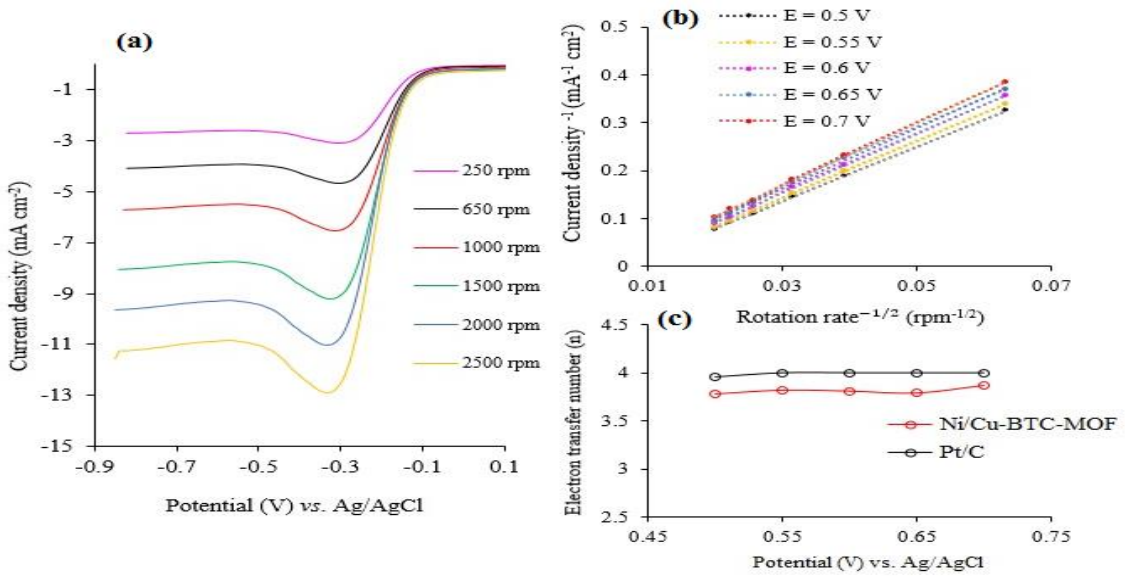

Figure 3. (a) LSV curves of Ni/Cu-BTC-MOF at different RDE rotational rates in 0.1mol L^{-1} KOH under saturated O_2 with a sweep rate of 10 mV s^{-1}, (b) The Koutecky Levich plots for the ORR on the Ni/Cu-BTC-MOF at different potentials, (c) Corresponding transferred electron numbers n

One major challenge to the construction of metal-air batteries is the durability of the electrocatalysts. The long-term durability of Ni/Cu-BTC-MOF and 20 wt. % Pt/C have been explored using chronoamperometric method in O_2-saturated 0.1 mol L^{-1} KOH solution at a rotation rate of 1600 rpm. As illustrated in Fig. 4a the current density for ORR on a modified electrode with Ni/Cu-BTC-MOF is approximately 85% of the initial current density after 10,000 seconds of continuous operation at a constant potential (-0.6 V vs. $Ag/AgCl/KCl_{sat.}$), while the current density for 20 wt.% Pt/C catalysts are about 71% of the initial current density at the same condition. This result indicates the acceptable durability of Ni/Cu-BTC-MOF for ORR. Furthermore, the resistance of the Ni/Cu-BTC-MOF to methanol crossover was studied by chronoamperometry measurement. According to Figure 4b, by

adding 1 mol L^{-1} of methanol the Ni/Cu-BTC-MOF demonstrates no apparent change but 20 wt. % Pt/C catalyst displayed a sharp decrease in current density due to the oxidation reaction of methanol at the same condition [44]. Therefore, it can be concluded the Ni/Cu-BTC-MOF catalyst has a high tolerance to methanol crossover.

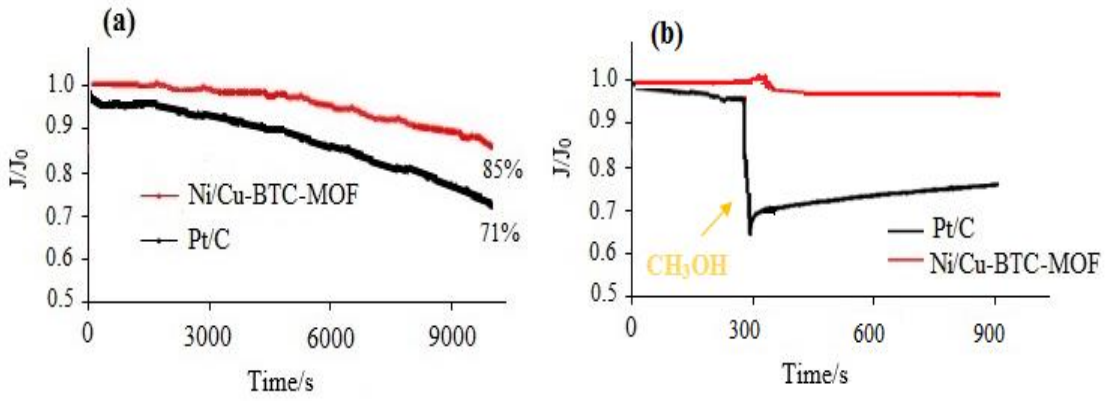

Figure 4. (a) *I–t* chronoamperometric stability responses for the ORR on Ni/Cu-BTC-MOF and Pt/C catalysts in O_2-saturated 0.1 mol L^{-1} KOH at -0.6 V (*vs.* Ag/AgCl) for the ORR at a rotating speed of 1600 rpm, (b) Methanol tolerance of on Ni/Cu-BTC-MOF and Pt/C

4. CONCLUSION

In summary, using an environmentally friendly, effective, and low-cost approach, Ni/Cu-BTC-MOF was synthesized and its electrochemical properties were examined using rotating disk electrode (RDE) tools. The Ni/Cu-BTC-MOF exhibits superior electrocatalytic properties of oxygen reduction reactions, in terms of onset potential, current density, durability, and tolerance to methanol. The outstanding electrocatalytic ORR behavior is due to the following aspects.

First, the porous framework and therefore the large specific surface area will improve the electrical conductivity of Ni/Cu-BTC-MOF. Second, this framework enhances effective sites to decrease the oxygen adsorption energy barrier and increase the adsorption capacity for oxygen molecules. The results clearly show that the Ni/Cu-BTC-MOF can be an appropriate alternative to precious platinum catalysts in metal-air batteries.

Acknowledgments

The authors would like to thank the University of Tehran for supporting this research financially.

Declarations of interest

The authors declare no conflict of interest in this reported work.

REFERENCES

[1] S. Chowdhury, and R. Balasubramanian, Prog. Mater. Sci. 90 (2017) 224.
[2] W. Wang, F. Lv, B. Lei, S. Wan, M. Luo, and S. Guo, Adv. Mater. 28 (2016) 10117.
[3] Y. Xu, M. Kraft, and R. Xu, Chem. Soc. Rev. 45 (2016) 3039.
[4] Y. Hao, Y. Xu, N. Han, J. Liu, and X. Sun, J. Mater. Chem. A 5 (2017) 17804.
[5] V. Calvaruso, and A. Craxı, Rsc. Adv. 5 (2015) 2.
[6] K. Sakaushi, and T.P. Fellinger, Chem. Sus. Chem. 8 (2015) 156.
[7] Y. Zha, K. Kamiy, K. Hashimot, and S. Nakanish, J. Phys. Chem. C 119 (2015) 2583.
[8] J. Mao, L. Yang, P. Yu, X. Wei, and L. Mao, Electrochem. Commun. 19 (2012) 29.
[9] H. Wang, M. Zhou, P. Choudhury, H. Luo, Appl. Mater. Today 16 (2019) 56.
[10] X. Yuan, HD. Sha, XL. Ding, HC. Kong, H. Lin, and W. Wen, Int. J. Hydrogen Energy 39 (2014) 15937.
[11] M. Sun, H. Li, Y. Liu, J. Qu, and J. Li, Nanoscale 7 (2015) 1250.
[12] K. Gong, P. Yu, L. Su, S. Xiong, and L. Mao, J. Phys. Chem. C 111 (2007) 1882.
[13] Z. Pu, Q. Liu, C. Tang, A.M. Asiri, AH. Qusti, and A.O. Al-Youbi, J. Power Sources 257 (2014) 170.
[14] D. Hu, H. Wang, J. Wang, Q. Zhong, Energy Technol. 3 (2014) 48.
[15] J.P. Collman, N.K. Devaraj, R.A. Decréau, Y. Yang, Y.L. Yan, W. Ebina, T.A. Eberspacher, and C.E. Chidsey, Science 315 (2007) 1565.
[16] M. Jahan, Z. Liu, and K. P. Loh, Adv. Funct. Mater. 23 (2013) 5363.
[17] B. Tang, S. Wang, R. Li, X. Gou, and J. Long, J. Power Sources 425 (2019) 76.
[18] V.R. Remya, and M. Kurian, Int. Nano Lett. 9 (2019) 17.
[19] W. Wang, Sci. Rep. 4 (2014) 5711.
[20] S. Liu, L. Sun, F. Xu, J. Zhang, C. Jiao, F. Li, Energy Environ Sci. 6 (2013) 818.
[21] M. Kurmoo, Chem. Soc. Rev. 38 (2009) 1353.
[22] T. Li-Li, L. Haiwei, Z. Yue, Z. Yuanyuan, F. Xiao, and W. Bo, Small 11 (2015) 3807.
[23] W. Cai, CC. Chu, and G. Liu, Small 11 (2015) 4806.
[24] Y. Cui, Y. Yue, G. Qian, and B. Chen, Chem. Rev. 112 (2011) 1126.
[25] S.L. James, Chem. Soc. Rev. 34 (2003) 276.
[26] J. Lee, O. K. Farha, J. Roberts, K.A. Scheidt, S.T. Nguyen, and J.T. Hupp, Soc. Rev. 38 (2009) 1450.
[27] B. Yuan, J. Zhang, R. Zhang, H. Shi, X. Guo, Y. Guo, X. Guo, S. Cai, and D. Zhang, Int. J. Electrochem. Sci. 10 (2015) 4899.
[28] Y.R. Lee, J. Kim, and W.S. Ahn, J. Chem. Eng. 30 (2013) 1667.
[29] A. Martinez Joaristi, J. Juan-Alcañiz, P. Serra-Crespo, F. Kapteijn, and J. Gascon, Cryst. Growth Des. 12 (2012) 3489.
[30] T.R. Van Assche, G. Desmet, R. Ameloot, D.E. De Vos, H. Terryn, and J. F. Denayer, Microp. Mesop. Mater. 158 (2012) 209.

[31] N. Campagnol, T. Van Assche, T. Boudewijns, J. Denayer, K. Binnemans, D. De Vos, J. Fransaer, J. Mater. Chem. A 1 (2013) 5827.
[32] M. Naseri, L. Fotouhi, A. Ehsani, and S. Dehghanpour, J. Coll. Interf. Sci. 484 (2016) 314.
[33] H. Pourfarzad, M. Shabani-Nooshabadi, M.R. Ganjali, J. Power Sources 451 (2020) 227768.
[34] H. Wang, F. Yin, B. Chen, and G. Li, J. Mater. Chem. A 3 (2015) 16168.
[35] U. Czaja, N. Trukhan, and U. Muller, Chem. Soc. Rev. 38 (2009) 1284.
[36] J. Hu, H. Yu, W. Dai, X. Yan, X. Hu, and H. Huang, RSC Adv. 4 (2014) 35124.
[37] T. Fan, F. Yin, H. Wang, X. He, and G. Li, Int. J. Hydrog. Energy 42 (2017) 17376.
[38] G. Xu, G.C. Xu, J.J. Ban, L. Zhang, H. Lin, C.L. Qi, Z.P. Sun, and D.Z. Ji, J. Colloid Interface Sci. 521 (2018) 141.
[39] C.L. Zhang, B.R. L, F.H. Cao, Z.Y. Wu, W. Zhang, H.P. Cong, and S.H. Yu, Nano Energy 55 (2019) 226.
[40] H. Zhang, H. Osgood, X. Xie, Y. Shao, and G. Wu, Energy 31 (2017) 331.
[41] C. Du, X. Gao, C. Cheng, Z. Zhuang, X. Li, and W. Chen, Electrochim. Acta 266 (2018) 348.
[42] X. Yang, X. Hu, X. Wang, W. Fu, X. He, T. Asefa, J. Electroanal. Chem. 823 (2018) 755.
[43] H. Tian, C. Zhang, P. Su, Z. Shen, H. Liu, G. Wang, S. Liu, and J. Liu, J. Energy Chem. 40 (2020) 171.
[44] D.M. Nguyen, M.H. Nguyen, and Q.B. Bui, J. Alloys Compd. 780 (2019)734.